S1 The Jenkinson-Collison automated Lamb Weather Typing Classification scheme

A 16 point grid is centered over the case study (Fig. S1). Based on the mean sea level pressure for this 16 point grid, the southerly, westerly and total component of the geostrophic surface flow and shear velocity are calculated.

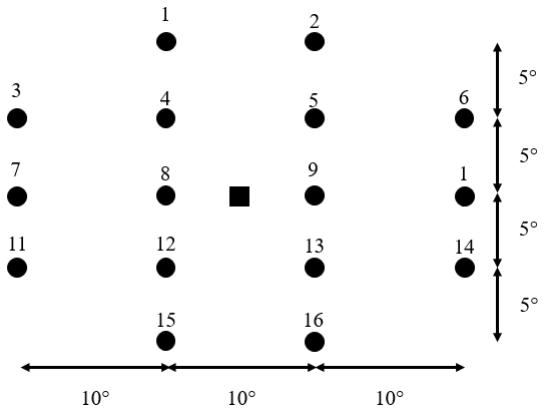

Figure S1 Spacing and numbering in the 16 point grid system for the Jenkinson-Collision automated Lamb weather typing classification scheme.

Assuming p_i is the pressure in point i of the 16 point grid, ψ the latitude of the case study/grid center (see ▪ in Fig. S1), then the southerly flow (SF), westerly flow (WF), total flow (F), southerly shear vorticity (ZS), westerly shear vorticity (ZW) and total shear vorticity (Z) are calculated following Eq. (S1).

$$WF = 0.5\,(p_{12} + p_{13}) - 0.5\,(p_4 + p_5)$$

$$SF = 1/\cos(\psi)\,[0.25\,(p_5 + 2\,p_9 + p_{13}) - 0.25\,(p_4 + 2\,p_8 + p_{12})]$$

$$F = (SF^2 + WF^2)^{1/2}$$

$$ZS = \sin(\psi) / \sin(\psi - 5)\,[0.25\,(p_6 + 2p_{10} + p_{14}) - 0.25\,(p_5 + 2\,p_9 + p_{13}) - 0.25\,(p_4 + 2\,p_8 + p_{12}) + 0.25\,(p_3 + 2p_7 + p_{11})] \quad \text{(S1)}$$

$$ZW = \sin(\psi) / \sin(\psi + 5)\,[0.5\,(p_{15} + p_{16}) - 0.5\,(p_8 + p_9)] - 1/2\,(\cos(\psi))^2\,[0.5\,(p_8 + p_9) - 0.5\,(p_1 + p_2)]$$

$$Z = ZS + ZW$$

The flow direction is calculated using Eq. (S2) and 45° sector is assigned for a 8 direction compass. If the outcome of Eq. (S2) is positive, 180° is added.

$$direction = 1 / \tan(\,WF / SF\,) \quad \text{(S2)}$$

Based on an inter-comparison of the flow indices (SF, WF, F, ZS, ZW and Z) and the flow direction, 27 different weather types (WTs) are identified. The inter-comparison of the flow indices considers following criteria:

- $|Z| < F$: pure directional WT (including 8 WTs according to the flow direction)
- $|Z| > 2F$ and $Z > 0$: pure cyclonic WT
- $|Z| > 2F$ and $Z < 0$: pure anti-cyclonic WT
- $F < |Z| < 2F$ and $Z > 0$: hybrid cyclonic WT (including 8 WTs according to the flow direction)
- $F < |Z| < 2F$ and $Z < 0$: hybrid anti-cyclonic WT (including 8 WTs according to the flow direction)
- $F < 6$ and $Z < 6$: undefined WT

S2 WT persistency

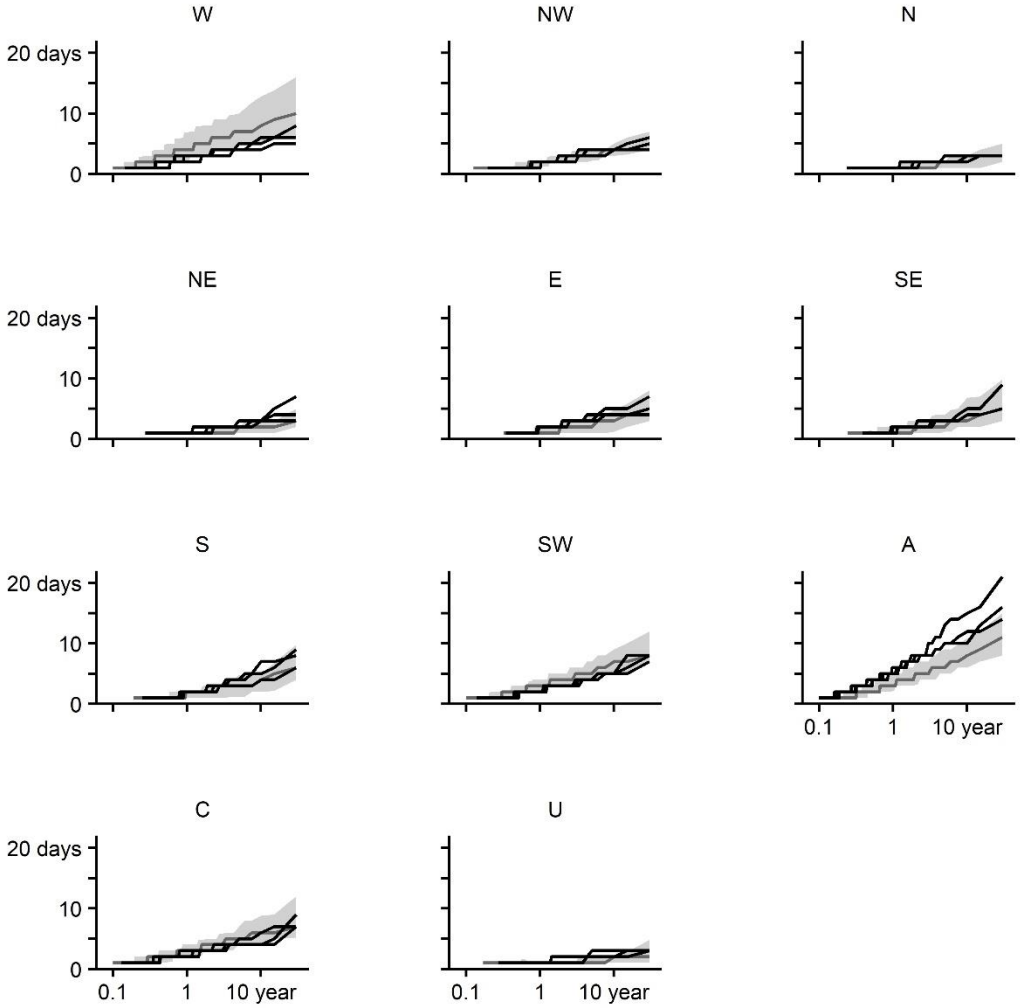

Figure S2 WT persistency during the winter season for different WTs and re-analysis datasets (black lines; EMULATE, ERA40, NCEP/NCAR) and climate model runs (grey line: median result, grey area: $5^{th} - 95^{th}$ percentile range of the results). The WT persistency is plotted in function of the empirical return period.

S3 Correlation between the bias and changes for the WT occurrences

Largest biases in the WT occurrences are found for the W and A WTs. In this section, we investigate the correlation between the bias and change. This correlation indicates the stationarity of the bias in the WToccurrences under increasing greenhouse gas scenarios. For this, the absolute values of the relative changes are plotted against the absolute values of the bias. Results for the RCP 8.5 sub-ensemble are shown in Fig. S3. For the W WTs, the larger biases (>10%) generally correspond with lower changes (< 15%). Futhermore, no significant differences are found across the re-analysis datasets. However, for the A WTs, most climate model runs with a larger bias (>15 %) project higher changes (>15%).

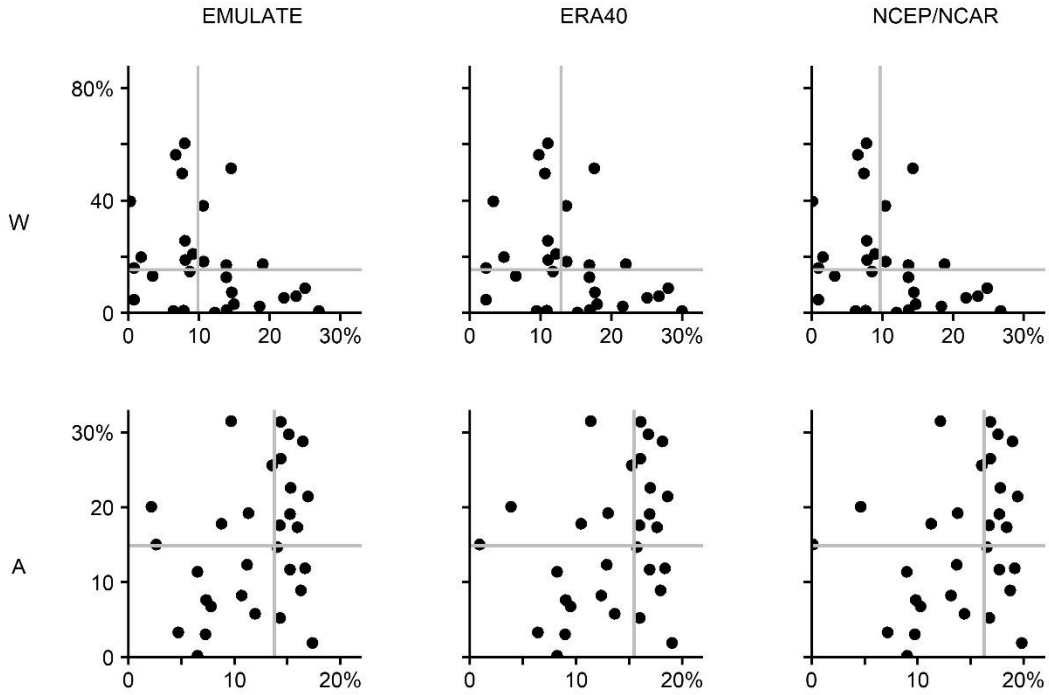

Figure S3 The absolute values of the relative change in the WT occurrences (vertical axis) in function of the absolute bias values (horizontal axis) for the RCP 8.5 climate model runs. The bias is defined as the absolute difference between the climate model and re-analysis dataset simulated occurrences for the period 1961-1990. The relative changes are based on the climate model output for 2071-2100 compared to the output for 1961-1990. The grey lines indicate the median change and bias for the RCP 8.5 sub-ensemble.

S4 The stationarity assumption

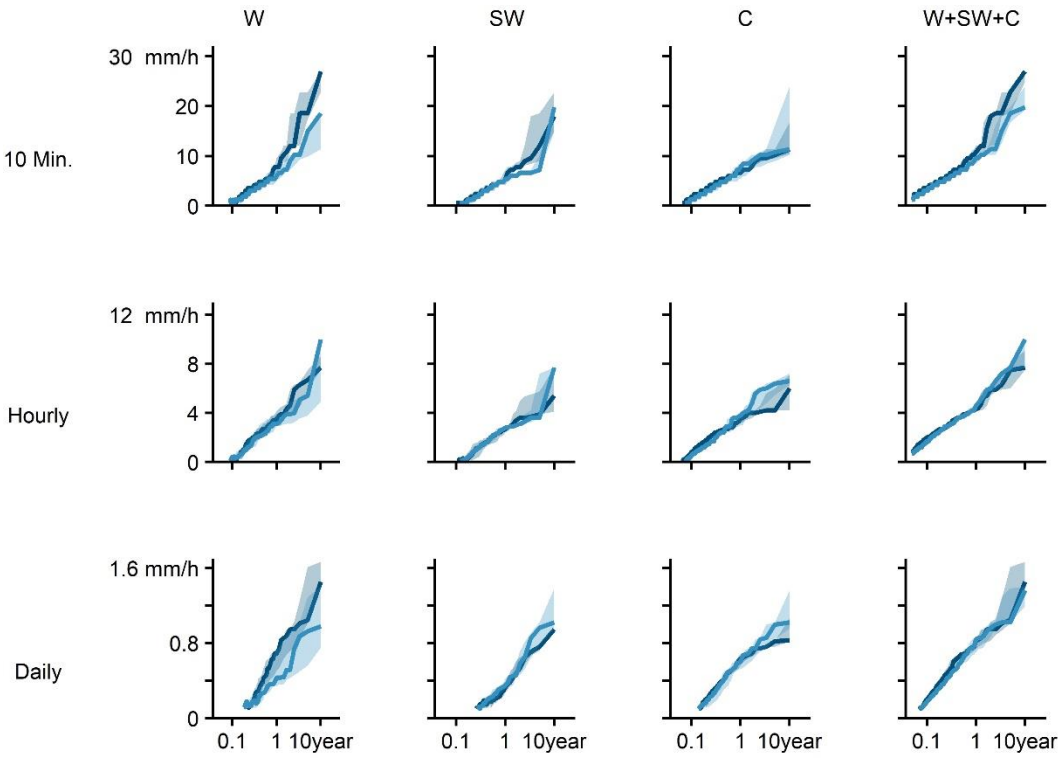

Figure S4 Independent 10 minutes, hourly and daily aggregated winter precipitation amounts associated with the wetter WTs. The precipitation amounts for moving windows starting between 1955 and 1965 are indicated by dark blue, whereas the light blue represent the amounts for moving windows starting between 1931 and 1941. The line shows the median result, whereas the colored area indicates the 5th to 95th percentile range.

S5 The perfect predictor experiment

The isolated skill of the Clausius-Clapeyron (CC) scaling is examined by comparing the perfect predictor experiment results for the original SDM (WT analogues and CC scaling) with the results for an adapted SDM version (WT analogues), for which the CC relation is turned off. The perfect predictor experiment results for the adapted version are shown in Fig. S5, Fig. S7 and Fig. S8 (left subfigure), whereas the results for the original version are shown in Fig. S6, Fig. S8 (right subfigure) and, Fig. 11 in the Manuscript.

Originally, analogues and re-sampling methods cannot produce predictand values outside the range of the calibration data. The relative change in the extreme 10 minutes precipitation amounts between the downscaled and calibration time series evolves therefore to 0% (no change) towards the highest return period (Fig. S5). However by including CC scaling in the downscaling methodology, the 0% change for the highest 10 minutes precipitation amount will not be developed (Fig. S6). By comparing Fig. S7 with Fig. 11 of the Manuscript, the effect of CC scaling appears in the reproduction of the precipitation extremes in the perfect predictor experiment. We note that the observations (black dots, 1991-2000) in these figures are not the calibration periods. In other words, the downscaled series cannot produce predictand values outside the range of the calibration data, but the predictand values of the calibration time series can be higher than the observed predictand values for 1991-2000. Furthermore, as indicated in the Manuscript, the prerequisites for analogue days restrict the number of corresponding historical days. Consequently the variance of the downscaled series will be underestimated (Fig. S8). Although the CC scaling was originally included to enable the extrapolation of the predictand values, it is found helpful to address the underestimated variance.

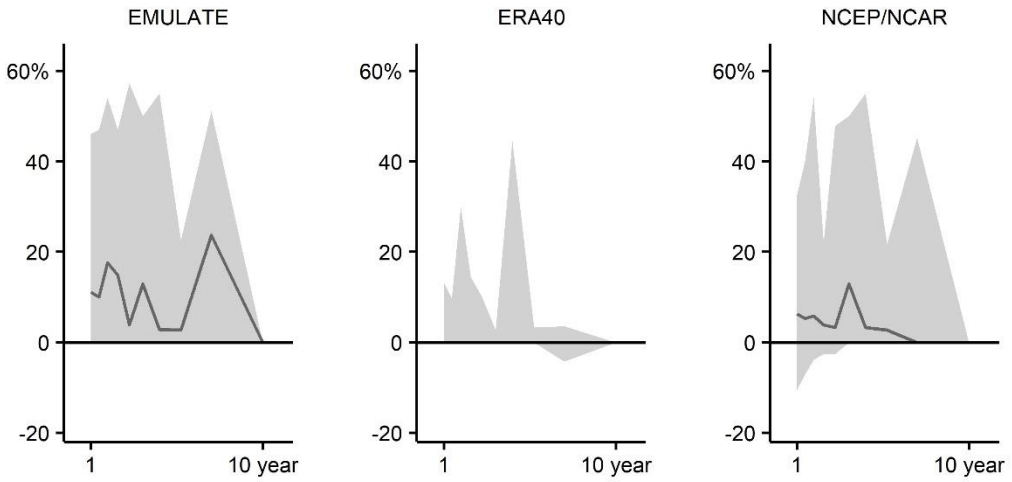

Figure S5 Relative change in the independent 10 minutes winter precipitation amounts between the downscaled and calibration time series. The downscaled series are obtained for the adapted SDM version, for which the CC scaling is turned off.

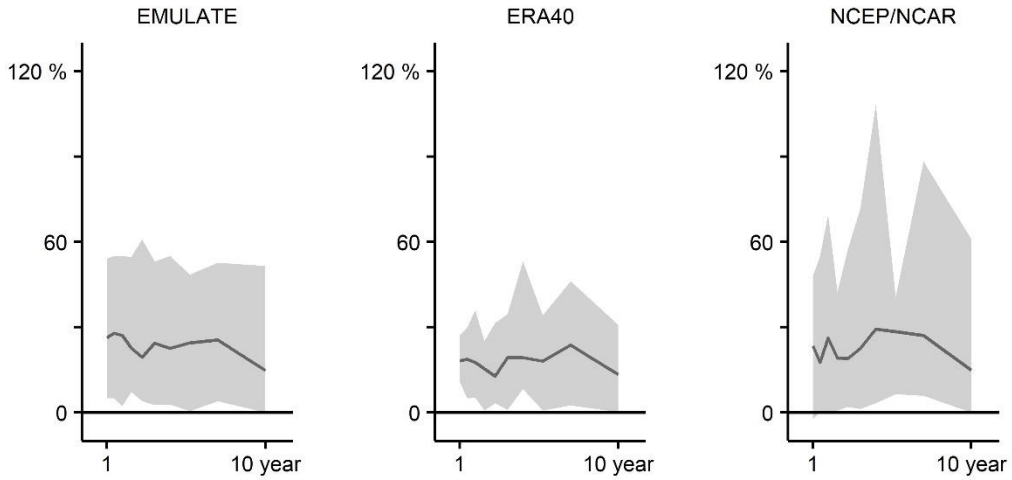

Figure S6 Relative change in the independent 10 minutes winter precipitation amounts between the downscaled and calibration time series. The downscaled series are obtained for the original SDM version, which combines WT analogues with CC scaling.

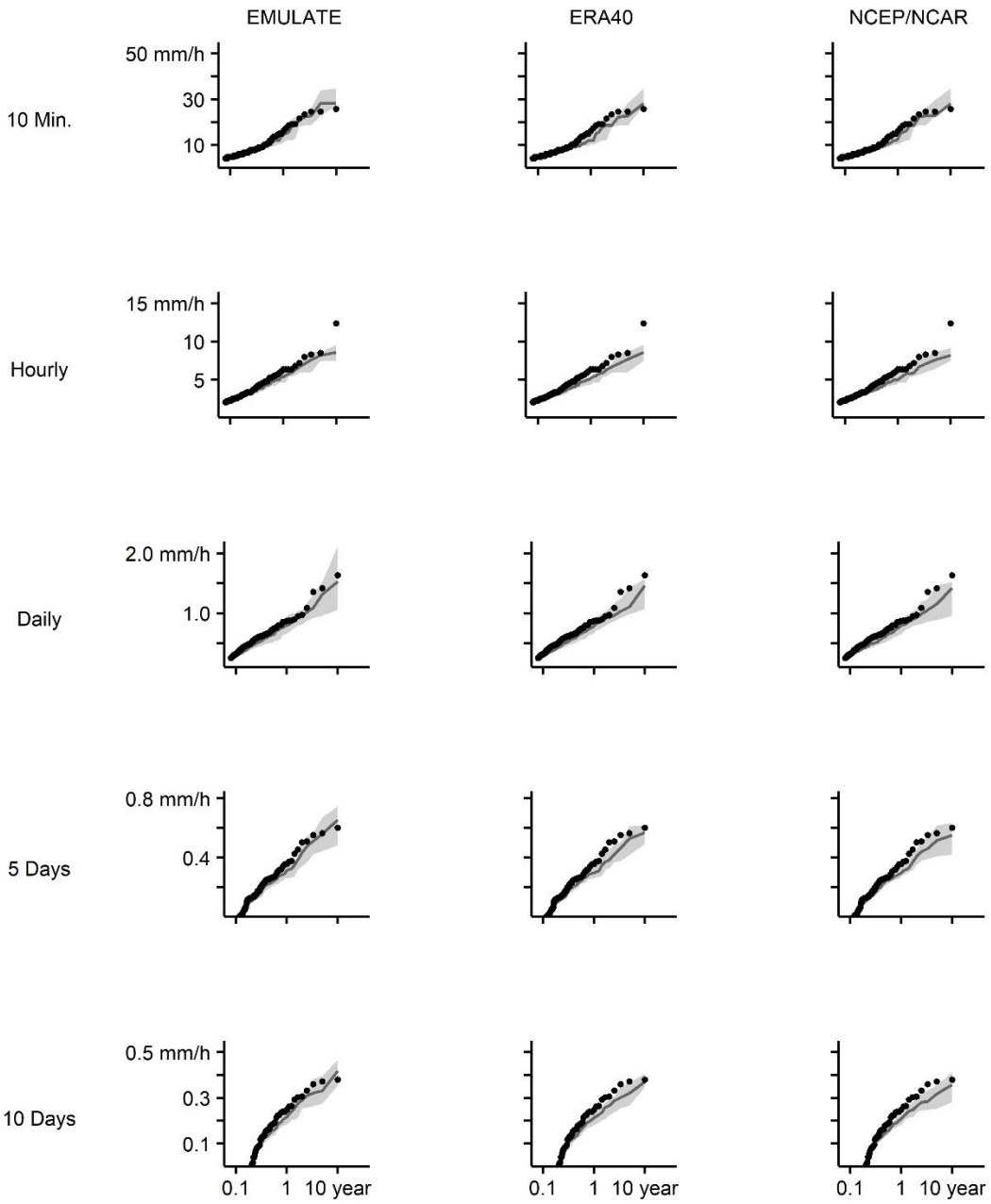

Figure S7 Independent winter precipitation amounts for the observed time series (black dots) and downscaled time series which are obtained in the perfect predictor experiment (grey line: median result, grey area: 5^{th}-95^{th} percentile of the results). The inter-comparison is made for different aggregation levels (rows) and re-analysis datasets (columns). The downscaled series are obtained for the adapted SDM version, for which the CC scaling is turned off.

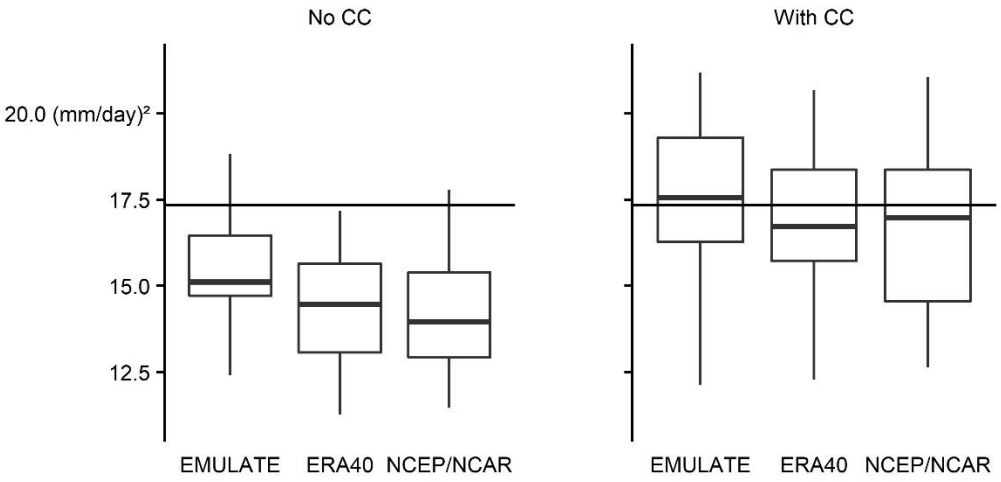

Figure S8 Variance of the daily winter precipitation amounts for the observed time series (horizontal line) and downscaled time series obtained in the perfect predictor experiment (boxplots). The downscaled series are obtained for the adapted SDM version, for which the CC scaling is turned off (left subfigure), and the original SDM version, which combines WT analogues with CC scaling (right subfigure).